RESEARCH ARTICLE

# Model-based control addition to prescribe DFIG wind turbine fast frequency response

**Nicholas David MS[1] | Thibault Prevost PhD[2] | Florent Xavier PhD[2] | Zhaoyu Wang PhD[1]**

[1]Electrical and Computer Engineering, Iowa State University, Ames, Iowa, 50011, USA

[2]Réseau de transport délectricité (RTE-France), 92073, Paris, La Defense, France

**Correspondence**
Nicholas David, Electrical and Computer Engineering, Iowa State University, 2520 Osborn Dr, Ames, IA, 50011, USA
Email: ndavid@iastate.edu

**Funding information**
Electric Power Research Center, Iowa State University; Power Systems Engineering Research Center (PSERC), Project S-73G

This paper investigates the physical capability of double-fed induction generator (DFIG) wind turbines for inertial support of frequency response. Frequency stability is modeled using the DFIG electromechanical and generator controller dynamics and a destabilizing effect is demonstrated in low-inertia systems. To improve response, a synchronous reference frame DFIG controller is proposed that acts by following low-frequency grid dynamics and adds a fast-acting PI-controlled frequency-responsive component to existing *qd* current commands. The proposed controller is derived in a straightforward manner using only the DFIG dynamic equations and is designed using pole/zero placement techniques. Laboratory experiments using a micro-scale DFIG wind turbine with hub-emulating flywheel prove better capability for transient frequency regulation even under extreme load change. The result is a DFIG controller that balances the appearance of transients in electrical and mechanical systems. Value is achieved in providing immediate continuous inertial response to support load change. The proposed frequency response can improve the use of existing physical inertia from wind turbines.

**KEYWORDS**
Flywheel, frequency control, inertia, wind energy generation, wind turbine generators, wind power control

## NOMENCLATURE

*Variables*

| | |
|---|---|
| $*$ | Control set-point command. |
| $e$ | In synchronous reference frame. |
| $'$ | Referred to stator using turns ratio. |
| $P_{s,\mathbf{sch}}$, $P_{s,\mathbf{act}}$ | Scheduled, actual generator power at stator. |
| $f_{e,\mathbf{sch}}$, $f_{e,\mathbf{act}}$ | Scheduled, actual electrical frequency. |
| $T_e$, $T_m$ | Electromagnetic, mechanical torque. |
| $P_s$, $P_r$ | Stator, rotor terminal power. |
| $P_{\mathbf{MPPT}}$ | Turbine power with maximum power point tracking. |
| $Q_s$ | Stator terminal reactive power. |
| $\theta_e$, $\theta_r$ | Stator voltage, rotor electrical angle. |
| $\omega_r$, $\omega_{rm}$ | Rotor electrical, mechanical speed. |
| $\omega_e$, $s$ | Stator electrical frequency, generator slip. |
| $v_{abcs}$ | Three phase stator voltage. |
| $i_{abcs}$, $i_{abcr}$ | Three phase stator, rotor current. |
| $v^e_{qs}$, $v'^e_{qr}$ | Stator, rotor $q$-axis voltage. |
| $v^e_{ds}$, $v'^e_{dr}$ | Stator, rotor $d$-axis voltage. |
| $i^e_{qs}$, $i'^e_{qr}$ | Stator, rotor $q$-axis current. |
| $i^e_{ds}$, $i'^e_{dr}$ | Stator, rotor $d$-axis current. |
| $\lambda^e_{qs}$, $\lambda'^e_{qr}$ | Stator, rotor $q$-axis flux. |
| $\lambda^e_{ds}$, $\lambda'^e_{dr}$ | Stator, rotor $d$-axis flux. |
| $T^*_e$, $Q^*_s$ | Torque, reactive power set-point. |
| $\omega^*_e$, $v^{e*}_{qs}$ | Frequency, voltage set-point. |
| $i'^{e*}_{qr,\mathbf{T}}$, $i'^{e*}_{dr,\mathbf{Q}}$ | Set-point by torque, reactive power control. |
| $i'^{e*}_{qr,\mathbf{F}}$, $i'^{e*}_{dr,\mathbf{V}}$ | Set-point by frequency, voltage control. |

*Parameters*

| | |
|---|---|
| $P$ | Number of generator poles. |
| $J$, $H$ | Physical, per-unit inertia. |
| $r_s$, $r'_r$ | Stator, rotor winding resistance. |
| $L_{ls}$, $L'_{lr}$ | Stator, rotor winding leakage inductance. |
| $L_M$ | Stator and rotor mutual inductance. |
| $L_s$ | Stator self inductance, $L_s = L_{ls} + L_M$. |
| $L'_r$ | Rotor self inductance, $L'_r = L'_{lr} + L_M$. |
| $s_{p\mathbf{T,Q}}$ | Poles of torque, reactive controllers. |
| $s_{z\mathbf{T,Q}}$ | Zeros of torque, reactive controllers. |
| $s_{p\mathbf{F,V}}$ | Poles of frequency, voltage controllers. |
| $s_{z\mathbf{F,V}}$ | Zeros of frequency, voltage controllers. |
| $K_{\mathbf{T}}$ | Proportional gain of torque control. |

| | |
|---|---|
| $\tau_T$ | Time constant of torque control. |
| $K_Q$ | Proportional gain of reactive power control. |
| $\tau_Q$ | Time constant of reactive power control. |
| $K_F$ | Proportional gain of frequency control. |
| $\tau_F$ | Time constant of frequency control. |
| $K_V$ | Proportional gain of voltage control. |
| $\tau_V$ | Time constant of voltage control. |
| $\tau_1$ | Current control filter time constant. |
| $\tau_2$ | TQ control filter time constant. |
| $\tau_3$ | FV control filter time constant. |
| $\tau_4$ | FV command filter time constant. |
| $\tau_5$ | MPPT command filter time constant. |
| $\tau_6$ | FV washout filter time constant. |

## 1 | INTRODUCTION

Decreasing inertia is one of the major obstacles to enabling very high penetration of renewable energy sources in future power systems. [1] Renewable energy resources with power electronic (PE) interface are reducing power system physical inertia and increasing susceptibility to voltage angle instability. [2,3] Wind turbines with a double-fed induction generator (DFIG) and PE back-to-back (B2B) converter are so-called "Type-III" machines. The power system is partially coupled to the massive rotor hub assembly by stator windings; the other portion is coupled to PE-connected rotor terminals. Wind turbines with DFIGs are a popular resource and may become the only source of electromechanical coupling between the power system and rotating mass. Their physical dynamics and control dynamics both influence their frequency response and their characteristics are critical to stability. This paper seeks to understand the problems associated with DFIG wind turbine frequency response and aims to improve the use of their physical inertia in frequency regulation.

Prior work in this field suggests that DFIGs possess sufficient capability for inertial frequency response when neglecting influence of control. [4] It is now hypothesized that through the flexibility of PE control, the DFIG can be made to offer its inertia to frequency response in an innovative and more effective way. This paper goes beyond generator modeling and evaluates the frequency response of DFIG control. Linearized transfer functions are derived using the DFIG dynamic model and its respective control laws. They reveal how conventional DFIG control action degrades the response. A PI controller is then derived from the DFIG dynamic model to correct and prescribe the frequency response.

A critical challenge is that PE controls, as they are today, require time to measure signals and process data before reacting to system change. This leads to a response delayed by tens to hundreds of milliseconds. As of today, synthetic inertia schemes use frequency measurement and cascaded control systems to react to system change, which is not immediate. A recent study suggests wind turbines with droop-type inertia emulation can be effective for up to 95 % penetration; the last 5 % being synchronous generation for inertia. [5] Although physical capability exists, today's controllers are insufficient for 100 % DFIG wind power. Effects from high penetration of droop-type wind turbine frequency response is observed in the Electric Reliability Council of Texas (ERCOT) power system, where wind is required to provide 5% frequency-droop if able to. Response there has improved "B-value" value (arrested stable frequency) but sometimes even lower "C-value" (nadir); the reason is unexplained. [6] In this paper, the influence that DFIG control has on its frequency response is considered and unstable effects are identified.

The art of DFIG wind turbine control has yet to achieve a mean of inertial fast frequency response (FFR). A gap

**TABLE 1** Attributes of select inertial frequency controllers

| Controller | General features | Fast inertial response | Signal acting on | Grid forming/following |
|---|---|---|---|---|
| [22] | Virtual rotor angle from proportionally controlled frequency with constant command $f^*$ | Y | $\theta_e - \theta_r$ | Form |
| [23] | Direct stator voltage control, virtual converter angle with constant $f^*$, no PLL | Y | $v_c^*$ | Form |
| [17] | Alters converter frequency, standalone with constant reference $f^*$, current $i^*$ from rotor speed control | Y | $\omega_e - \omega_r$ | Form |
| [18] | Applies droop, ROCOF, sub-opt MPPT, and speed control to one torque command | N | $T_e^*$ | Follow |
| [10] | GE's WindINERTIA; cascaded and uses droop gain based on available power, includes washout filter | N | $P^*$ | Follow |
| [7] | Wind linked by HVDC with VSC, frequency response linked to physical $J$ via B2B converter, adds integral control of frequency | N | $P^*$ | Follow |
| [24] | Uses 2 PLLs – one fast for inertial response, multiplies $i^*_{MPPT}$ with an I-f droop | Equal | $i^*$ | Follow |
| [25] | Offshore wind with DC-link and VSC, links $f_e$ to physical $J$ via B2B, GSC alters $v_{dc}$ and MSC translates $v_{dc}$ to additional $P^*$ | N | $v^*_{dc}$, $P^*$ | Follow |
| [26] | Offshore wind with HVDC and VSC, links $f_e$ to physical $J$ via B2B, I-f droop acts directly on $v_c^*$ added through a LPF with constant $f^*$ | Y | $v_c^*$ | Form |
| NEW | Follows low-frequency grid dynamics, PI controller adds to $i^*_{MPPT}$, control easily designed seperately from and to be faster than TQ control, washout filter limits impact, simple PLL | Y | $i^*$ | "Driving" |

exists in knowledge of response capability and opportunities exist to enhance inertial response via novel control techniques. A range of DFIG wind turbine steady-state, primary, and secondary controls are available in literature and range in complexity and performance. [7–13] A selection of these and other DFIG wind turbine controllers proposed for inertial frequency response are summarized for their general qualities and performance capability in Table 1. Other controllers operate on torque or power commands with slow cascaded control and may have operating power headroom requirements. [10,14–20] A direct voltage and frequency control adjusting voltage commands can provide fast response but current harmonic distortion can increase. [21] A controller using trajectory generation to replace vector control has also been proposed but requires coordination with other sources via communication. [16]

The contribution of this paper is a PI-type frequency and voltage (FV) control addition to expand the DFIG inertial response capability. It draws on elements of the existing art by operating on current commands to maintain harmonic integrity, using a wash-out filter to limit low-frequency response, and using PE control to link the physical inertia to the electrical frequency response. It is innovative in that it provides a fast-acting response to load change while also following low frequency grid dynamics in a way that is designed and specified. Additionally, it uses only local measurements and does not require communication. It adds a transient-only component to the existing torque and reactive power controllers. Furthermore, FV and TQ controllers are designed independently using only the DFIG dynamic model. The new (inertial) and existing (steady-state) controllers are made to complement each other with ability to tune intensity and duration of frequency response. Capability of sustained support is limited by the physical inertia and is driven by the controller design. A fundamental novelty of this work lies in thinking of the DFIG as a hybrid "grid-driving" (not just grid-"forming" or "following") resource with loose and controlled stator frequency.

Specific objectives of this paper are to 1) provide analytic and experimental evidence about frequency stability of DFIG wind turbines in low-inertia power systems, 2) derive torque control influence on frequency stability in response to load step-change, 3) propose and derive a new inertial load-responsive DFIG controller to complement existing controls and improve wind turbine utility, 4) perform experiments to demonstrate the utility-connected and islanding-mode inertial frequency response using a micro-scale DFIG wind turbine emulator (rated 7.5 kW) equipped with a hub-emulating rotor flywheel.

The remainder of this paper is organized to illustrate the issues. Section 2 first explains principles of DFIG wind turbine-based power systems, modeling the DFIG and control dynamics and identifying problems in the frequency stability. Section 3 proposes a novel controller to correct and prescribe the inertial response. Experiments in Section 4

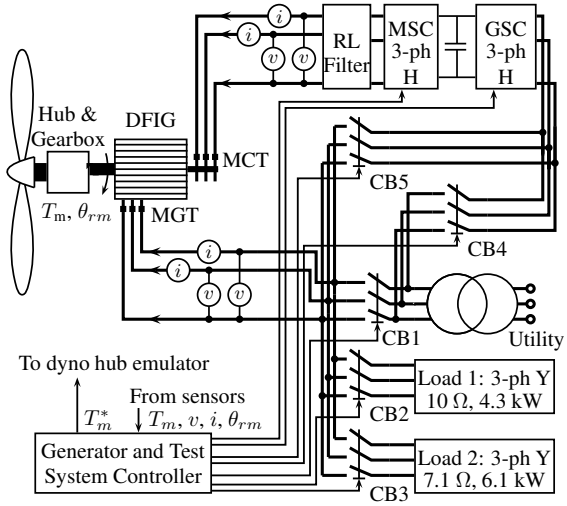


**FIGURE 1** High-level schematic of a DFIG-based local power system for utility-connected or islanded operation.

demonstrate the proposed wind turbine inertial capability and proves that effective utility-integrated and islanding response can be had from DFIG wind turbine inertia. Conclusions regarding the capability of DFIG wind turbines to contribute their inertia to frequency response are provided in Section 5.

## 2 | FREQUENCY PROBLEMS IN LOW-INERTIA DFIG POWER SYSTEMS

Effects of interconnecting PE-controlled low-inertia generators on power system frequency response is not widely understood. The difficulty is that sufficient physical inertia must exist to maintain frequency during the sensing, detecting, activating, and start of primary response; on the scale of tens to hundreds of milliseconds. Most critical to the response characteristic is the way in which the DFIG is controlled. This section discusses fundamentals of the DFIG in low-inertia power systems and derives the problem of DFIG frequency instability.

### 2.1 | Preliminaries of modeling the DFIG frequency response

A realistic power system that can be used to evaluate DFIG wind turbine frequency response is illustrated in Figure 1. The hub and gearbox rotating mass are emulated in the laboratory by a rotor flywheel and driven by a dynamometer. Connection to the local utility power system is made via CB1 and a variac autotransformer. Resistive loads are connected at the stator-side of circuit breaker CB1 via CB2 and CB3. The DFIG is controlled by a machine-side converter (MSC) while a grid-side converter (GSC) regulates the dc-link voltage and the reactive power at the GSC terminals. CB4 and CB5 allow GSC influence to be either neglected or considered in the tested response. Generator control relies on voltage and current sensing at the machine-grid terminal (MGT) and current sensing at the machine-converter terminal (MCT). Current is defined positive into the machine. It is assumed that utility generation is composed of additional sources that provide inertial, primary, and secondary response, such as synchronous generators, PE-connected photovoltaics, energy storage systems, and other wind turbines. Opening CB1 with CB4 open and CB5 closed makes the load fully reliant on the DFIG and PE converters without support from the grid.

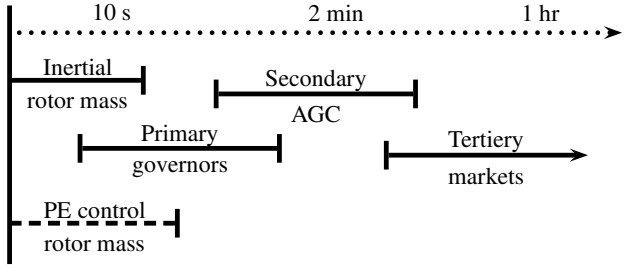


**FIGURE 2** Relative power system frequency response periods; the PE-driven response proposed in this paper resides in a region indicated by the dashed line.

Frequency response is well-defined by the North American Electric Reliability Corporation (NERC). [27] Illustrated in Figure 2, there are four periods in which to consider response. Each has requirements met by appropriate resources and response methods including inertia, governors, and automatic generation control (AGC). [28,29] Response characteristics that are "inertial", "immediate", "bi-directional", "continuous", and "sustained" are considered valuable and essential. The DFIG controller proposed in this paper exhibits these qualities. It acts continuously in the inertial period indicated by the dotted line.

In the U.S.A., NERC performance standards guide design and operation of generation equipment. NERC Standard BAL-001-2 aims to keep transmission interconnection frequency within defined limits. [30] It also provides performance calculation of area control error (ACE). In this paper generator contribution to frequency response is measured using a similar performance measure

$$\text{ACE}\Delta f = (P_{s,\text{sch}} - P_{s,\text{act}})(f_{e,\text{act}} - f_{e,\text{sch}}). \tag{1}$$

Providing $\text{ACE}\Delta f < 0$ kW $\cdot$ Hz contributes to regulation; the DFIG controller proposed in this paper exhibits this behavior. Frequency nadir is another response event attribute that is impacted by the proposed control.

In this paper, frequency is measured using a synchronous reference frame phase-locked loop (SRF-PLL), which is already used for normal DFIG operation. [31] The PLL operates by accelerating the reference frame angle to keep $v^e_{ds} = 0$ V. The PLL controller is tuned for a voltage angle-step response which is much faster than the current controller step response, as a virtue of cascaded control; it has negligible impact on the frequency response.

Generator rotor speed and torque are linked by the swing equation

$$\frac{2}{P} J \frac{d\omega_r}{dt} = T_e + T_m - D\omega_r, \tag{2}$$

where $D$ is mechanical damping and $T_m$ is the mechanical torque applied by the wind and which is assumed constant in the duration of interest. Polarity of torque and speed are defined such that applying $T > 0$ accelerates $\omega > 0$. It is assumed that $T_m$ corresponds to electrical rotor speed, $\omega_r$, for maximum power point tracking (MPPT). [8] Electrical dynamics and MSC control both influence electromagnetic torque $T_e$.

The DFIG electromagnetic dynamic model has been derived for the synchronous reference frame (SRF). [32] It is normally applied under the assumption of a stiff grid, i.e. constant stator frequency. An important factor in this paper is that this assumption is relaxed so that $d\omega_e/dt = d\omega_r/dt$. This means the DFIG is driving the system.

Per-unit inertia, $H$, has units of s (seconds), whereas physical inertia, $J$, has units of kg $\cdot$ m$^2$. The two are related by

$J = S_b H P^2/(2\omega_b^2)$, where $S_b$ is the per-unit generator power base ($S_{\text{rated}}$) and $\omega_b$ is the power system angular frequency base ; here, $\omega_b = 2\pi 60$ rad/s. Thermal synchronous generators have $H \approx 6$–12 s, whereas DFIG wind turbines have $H \approx 2$–3 s. PV and ESS have $H = 0$ s. In systems with low inertia $\omega_e$ is more inclined to accelerate; it cannot be considered constant.

Electrical power in the DFIG is split between stator and rotor terminals and related to mechanical shaft power and speed by

$$P_s = \frac{-P_m}{1-S}, \tag{3}$$

$$P_r = -SP_s, \tag{4}$$

where slip, $S$, is defined as

$$S = \frac{\omega_e - \omega_r}{\omega_e}. \tag{5}$$

$T_e < 0$, $P_s < 0$, and $P_r < 0$ imply electrical generation. The MSC operates with a frequency of $\omega_e - \omega_r$ by virtue of PLL-based SRF control.

DFIG torque, reactive power, and current control are normally derived from the DFIG dynamic equations.[8] Each uses proportional plus integral (PI) current control laws designed in the Laplace domain to form stable linear time-invariant systems. The current control is designed to have a relatively fast current-step response so its contribution to frequency response is negligible. Space vector modulation (SVM) of the SRF voltage commands creates the switching signals that drive the MSC.

Current commands normally originate from torque and reactive power (TQ) controllers as

$$i'^{e*}_{qr,\text{T}} = \frac{\lambda^e_{qs} i'^e_{dr}}{\lambda^e_{ds}} + \left(T_e - T^*_e\right) K_\text{T}\left(1 + \frac{1}{\tau_\text{T} s}\right), \tag{6}$$

$$i'^{e*}_{dr,\text{Q}} = \frac{\lambda^e_{ds}}{L_M} + \left(Q_s - Q^*_s\right) K_\text{Q}\left(1 + \frac{1}{\tau_\text{Q} s}\right). \tag{7}$$

Note that a more positive q-axis current creates more negative (generating) torque. Parameters $K_{\text{T,Q}}$, $\tau_{\text{T,Q}}$ achieve specified TQ closed-loop transfer function poles and zeros. Using cascaded control, TQ control is designed to be relatively slow compared to current control. Frequency and voltage droop-type controls normally alter the TQ set-point commands in a cascaded way, thus limiting the rate of transient response capability.

The next subsection illustrates how the conventional control scheme promotes instability and is insufficient for use in DFIG-driven power systems. Following that is a new control method proposed to counteract those effects and correct the response by design.

## 2.2 | Instability of the DFIG in low-inertia power systems

Action of the TQ controllers is the source of the problem. Consider a real load increase that appears as a voltage angle step. The SRF-PLL tracks the angle change, thus transient appears in the measured frequency, *qd* current, and electromagnetic torque. Current and torque have an apparent step-change, and frequency an impulse. Measurement of $\Delta T_e$ creates an equivalent $-\Delta T^*_e$. The problem is that the torque control is made to have constant torque, while this is not what is expected in a low-inertia grid. The torque controller responds to the apparent torque change by reducing

the current command. The effect is that this actually reduces $T_e$ in response to the load increase; opposite of the desired response.

Proof and mechanisms of instability are revealed by the linearized dynamic model. To link effects of physical inertia and controller influences, (2) is used with $T_e$ written in terms of $qd$ current and flux. With fast current control, one can assume $i'^e_{qr} = i'^{e*}_{qr}$ and $i'^e_{dr} = i'^{e*}_{dr}$. The resulting swing equation is

$$\frac{2J}{P}\frac{d\omega_e}{dt} = \left(\frac{3P}{4}\right)\left(\frac{\lambda^e_{ds}\lambda^e_{qs}}{L_s} - \frac{\lambda^e_{ds}L_M}{L_s}i'^{e*}_{qr} - \frac{\lambda^e_{qs}\lambda^e_{ds}}{L_s} + \frac{\lambda^e_{qs}L_M}{L_s}i'^{e*}_{dr}\right) + T_m - D(1-S)\omega_e. \tag{8}$$

Including TQ controller influence of (6) and (7), and assuming $\lambda^e_{ds} \approx v^e_{qs}/\omega_e$ and $\lambda^e_{qs} \approx 0$, then

$$\frac{2J}{P}\frac{d\omega_e}{dt} = -\frac{3Pv^e_{qs}L_M}{4L_s}\omega_e^{-1}T_e\left(K_\mathrm{T} + \frac{K_\mathrm{T}}{\tau_\mathrm{T}s}\right) + \frac{3Pv^e_{qs}L_M}{4L_s}\omega_e^{-1}T^*_e\left(K_\mathrm{T} + \frac{K_\mathrm{T}}{\tau_\mathrm{T}s}\right) + T_m - D(1-S)\omega_e. \tag{9}$$

Equation (9) means that the control parameters $K_\mathrm{T}$ and $\tau_\mathrm{T}$ act together with inertia, $J$, to influence the frequency response. It affords building a transfer function to study frequency response due to apparent change of torque command, $H(s) = \Delta\omega_e(s)/\Delta T^*_e(s)$.

Linearizing (9) about the operating point, the partial derivatives $df(\omega_e, T^*_e) = (\partial f/\partial\omega_e)d\omega_e + (\partial f/\partial T^*_e)dT^*_e$ are

$$\frac{\partial f}{\partial \omega_e} = -D(1-S), \tag{10}$$

$$\frac{\partial f}{\partial T^*_e} = \frac{3Pv^e_{qs}L_M}{4L_s\omega_e}\left(K_\mathrm{T} + \frac{K_\mathrm{T}}{\tau_\mathrm{T}s}\right). \tag{11}$$

Therefore, the linearized swing equation in the Laplace domain is

$$\frac{2J}{P}s\Delta\omega_e = -D(1-S)\Delta\omega_e + \frac{3Pv^e_{qs}L_M}{4L_s\omega_e}\left(K_\mathrm{T} + \frac{K_\mathrm{T}}{\tau_\mathrm{T}s}\right)\Delta T^*_e \tag{12}$$

and the transfer function is

$$\frac{\Delta\omega_e}{\Delta T^*_e} = \frac{3P^2v^e_{qs}L_MK_\mathrm{T}}{8JL_s\omega_e}\frac{\left(s + \frac{1}{\tau_\mathrm{T}}\right)}{s\left(s + \frac{D(1-S)P}{2J}\right)} \tag{13}$$

with $v^e_{qs}$, $\omega_e$, and $S$ evaluated at the initial operation condition. The system has one zero at $s_{z,\mathrm{T}} = -1/\tau_T$, one pole at $s_{\mathrm{p1,T}} = 0$, and a second pole at $s_{\mathrm{p2,T}} = -D(1-S)/(2J)$. The system is unstable with $J$, $K_\mathrm{T}$, and $\tau_\mathrm{T}$ contributing to the magnitude and phase of response. The damping, $D$ is usually small and a matter of physical design (e.g. the laboratory DFIG system has $D = 2.74 \times 10^{-4}\mathrm{kg}\cdot\mathrm{m}^2\mathrm{rad}^{-1}\mathrm{s}^{-1}$) making the second pole also close to the origin. Slowing torque controller $\tau_\mathrm{T}$ can improve response by moving the zero, but cannot practically be made slow enough.

Adequacy of the time-domain DFIG frequency response is evaluated by simulating an islanding operation with a local stator-connected resistive load in a configuration similar to that of Figure 1. Consider the utility-connected wind turbine near rated MPPT power with $Q_s = 0$ var and local resistive load consuming 10 % more power than being produced at the stator. To neglect the GSC influence on response, the GSC is connected with CB4 closed and CB5 open. When the utility connection is opened via CB1 the turbine stator is then 10 % overloaded and the frequency response at the load is entirely dependent on the DFIG. The simulated inertial response in Figure 3 illustrates the degrading effect of the control designs listed in Table 2. Proof of load-supporting inertial frequency response shall coincide with

**TABLE 2** Simulated TQ control designs and their inertial frequency response

| Control designs | | | | | Frequency response results | | | |
|---|---|---|---|---|---|---|---|---|
| | Set | $\tau_2$ (ms) | $s_{pT,Q}$ (rad/s) | $s_{zT,Q}$ (rad/s) | $f_{e,\text{nadir}}$ (Hz) | $t_{\text{nadir}}$ (ms) | $f_{e,\text{t=0.2 s}}$ (Hz) | Comment |
| A | Fast | 22.7 | -60, -20 | -30, -40 | 54.53 | 24.9 | 215.6 | Most quickly unstable |
| B | Slow | 22.7 | -6, -2 | -3, -4 | 53.81 | 30.9 | 87.67 | Instability is slowed |
| C | Slower | 22.7 | -0.6, -0.2 | -0.3, -0.4 | 53.72 | 31.9 | 76.87 | Instability is slowed more |
| D | Damped | 22.7 | -5.1, -2 | -0.6, -20 | 52.01 | 40.5 | 58.65 | Instability is slowed much more |
| E | Filtered | 227 | -1, -2 | -0.5, -4 | 36.31 | 377.4 | 41.22 | Instability is almost benign |
| F | Drooped | 22.7 | Case E + 5 % droop | | 54.2 | 20.9 | 57.7 | Oscillation in response |

observation of more negative $T_e$ and $\Delta\omega_{rm} < 0$.

Cases A–D are TQ-only control and show decline in $|T_e|$ and $\Delta\omega_{rm} > 0$ rpm, which means they actually respond with inertial load rejection instead of load support. The load-loss creates an apparent torque increase that initiates controller response and leads to instability. Case E has less torque loss during this period from the use of a slower low-pass filter, $\tau_2$, on the TQ control elements. Control speed (pole placement) and low-pass filtering effects the duration and intensity of the frequency response. Case F applies a 5 % frequency-droop control. Some inertial contribution is observed in $\Delta\omega_{rm}$ but with unacceptable oscillations in $f_e$.

Conventional DFIG controls do not provide a frequency response that is adequate for 100 % reliance during load-transient. Problems arise in stability due to effect of controls that are not intended for use in loose-grid and self-supporting operation modes. A DFIG controller is proposed in the next section to correct the frequency response and link the electrical load-transient to the physical energy reserve in the mechanical rotor.

## 3 | PROPOSED DFIG FREQUENCY AND VOLTAGE CONTROL

The proposed DFIG control solution counteracts the destabilizing effects of TQ control. It adds a transient-only component of current command to provide prescribed grid-following frequency and voltage regulation. The proposed control addition easily integrates with the existing steady-state TQ controller and links load transients to rotor speed deviation. Parameters of the design change how $J$ appears in the frequency response. A schematic of the DFIG controller is drawn in Figure 4 with the new component highlighted in dashed lines. No change to the existing TQ controller is necessary.

Proposed is a second set of PI-controlled current commands that are added to those of (6) and (7). Instead of controlling only the frequency, the frequency and voltage are both controlled because they quantify the speed and magnitude of the one electromagnetic field that is driving the load. The FV control design is based only on generator parameters and can be tuned for desired response. A high pass filter (HPF) limits bandwidth of the FV response, allowing only temporary excursion from normal TQ operation to support load change. Commands $f_e^*$ and $v_{qs}^{e*}$ are obtained from LPF stator measurement so the DFIG follows slower grid dynamics. The proposed controller does not provide targeted value of apparent inertia, but rather acts to regulate frequency via energy exchange with the rotor mass. It provides a tunable balance of transient appearance in mechanical and electrical dynamics.

The proposed control laws are derived using only the DFIG dynamic equations.[32] Current commands $i'^{e*}_{qr,\text{F}}$ and $i'^{e*}_{dr,\text{V}}$ are derived from the voltage equations using PI control law to form linear time-invariant functions. The current

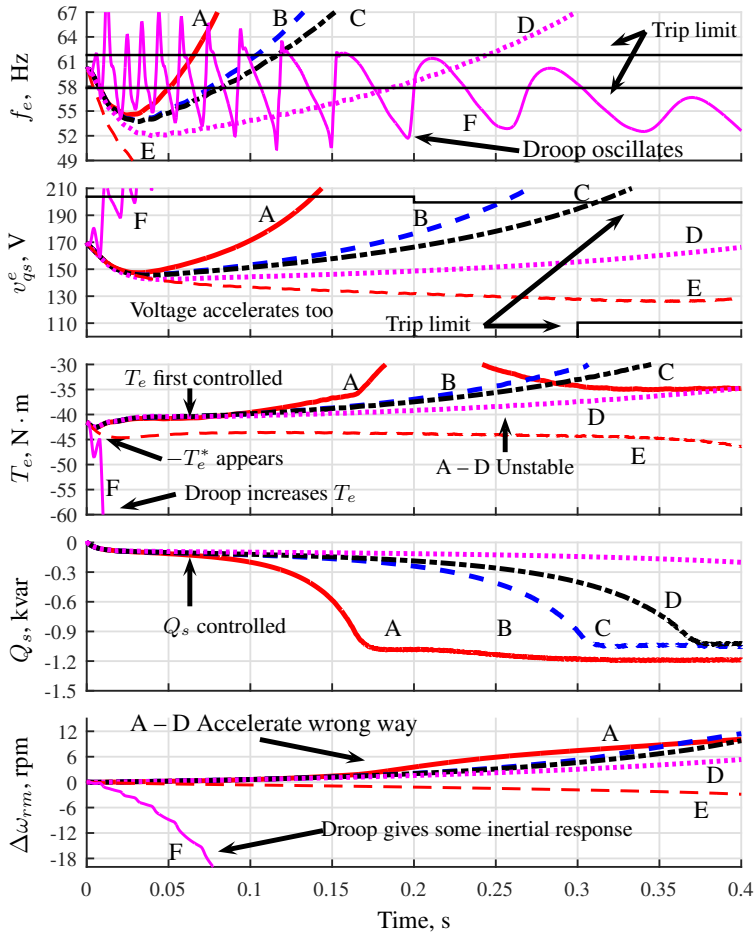


**FIGURE 3** Inertial response to a 10 % load increase with 100 % reliance on DFIG inertial frequency response. Plotted are TQ-only control designs made fast (A, solid), slow (B, dashed), slower (C, dot-dashed), slow with high damping (D, dotted), slow with lower filter (E, thin dashed), and with 5 % droop (F, oscillating solid).

commands are thus defined as

$$i'^{e*}_{qr,\mathrm{F}}(\omega_e) = \left(\omega^*_e - \omega_e\right) K_\mathrm{F}\left(1 + \frac{1}{\tau_\mathrm{F} s}\right) + \frac{r_s i^e_{ds}}{\omega_e L_M} - \frac{v^e_{ds}}{\omega_e L_M} - \frac{v^e_{qs} L_s}{r_s L_M}, \tag{14}$$

$$i'^{e*}_{dr,\mathrm{V}}(v^e_{qs}) = \left(v^{e*}_{qs} - v^e_{qs}\right) K_\mathrm{V}\left(1 + \frac{1}{\tau_\mathrm{V} s}\right) - \frac{r_s i^e_{qs}}{\omega_e L_M} - \frac{i^e_{ds} L_s}{L_M}. \tag{15}$$

The FV control laws can be used alone in a grid-forming mode or combined with others to obtain good effect as done in this paper. Notice that the FV control law is not impacted or limited by the TQ design; this is not the case with cascaded

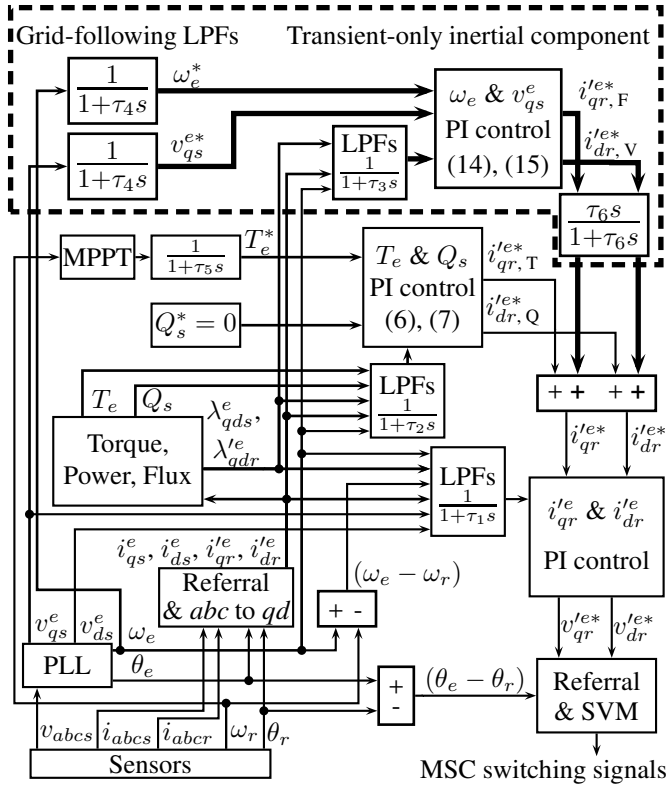


**FIGURE 4** Proposed transient-only FV control addition (dashed outline) to complement existing steady-state controllers.

controls. Gains $K_{\mathrm{F,V}} > 0$ and time constants $\tau_{\mathrm{F,V}} > 0$ s are designed with

$$K_{\mathrm{F}} = \frac{\frac{s_{p\mathrm{F}}}{s_{z\mathrm{F}}} L_s \lambda^e_{ds}}{\left(1 - \frac{s_{p\mathrm{F}}}{s_{z\mathrm{F}}}\right) r_s L_M}, \tag{16}$$

$$K_{\mathrm{V}} = \frac{\frac{-s_{p\mathrm{V}}}{s_{z\mathrm{V}}}}{\left(\frac{s_{p\mathrm{V}}}{s_{z\mathrm{V}}} - 1\right) \omega_e L_M}, \tag{17}$$

$$\tau_{\mathrm{F,V}} = \frac{-1}{s_{z\mathrm{F,V}}}, \tag{18}$$

to place the pole and zero of the respective closed-loop transfer functions, which are

$$\frac{\omega_e(s)}{\omega_e^*(s)} = \frac{K_{\mathrm{F}}(\tau_{\mathrm{F}} s + 1)}{\left(\frac{L_s \lambda^e_{ds}}{r_s L_M} + K_{\mathrm{F}}\right) \tau_{\mathrm{F}} s + K_{\mathrm{F}}} \tag{19}$$

$$\frac{v^e_{qs}(s)}{v^{e*}_{qs}(s)} = \frac{(K_{\mathrm{V}} \tau_{\mathrm{V}} s + K_{\mathrm{V}})}{(K_{\mathrm{V}} + 1/(\omega_e L_M))\, \tau_{\mathrm{V}} s + K_{\mathrm{V}}}. \tag{20}$$

Placing the poles, $s_{pF,V}$, and zeros, $s_{zF,V}$, in the left half plane with $s_{pF,V}/s_{zF,V} < 1$ provides stable response.

Since both TQ and FV controls operate on the same current command, it can be possible for them to interfere. However, their respective individual transfer functions can be designed to mitigate interference. In fact FV response can be made fast enough to provide reliable stability and with low-frequency response washed out in order to follow slower dynamics with TQ response. Effect of the combined TQ and FV control on the inertial frequency response can be derived in a way similar to (13). The linearized transfer function proves the stabilizing properties of the proposed control addition. The resulting transfer function is

$$\frac{\Delta\omega_e}{\Delta T_e^*} = \frac{\frac{\alpha K_T}{\omega_e}\left(s+\frac{1}{\tau_T}\right)\left(s+\frac{1}{\tau_6}\right)}{\frac{2J}{P}s^3+\left(\frac{2J}{P\tau_6}+\gamma+\frac{\alpha v_{qs}^e L_s}{\omega_e^2 r_s L_M}\right)s^2+\left(\frac{\gamma}{\tau_6}-\frac{\alpha K_F}{\omega_e}\right)s-\frac{\alpha K_F}{\omega_e \tau_F}}. \tag{21}$$

where $v_{qs}^e, \omega_e, \alpha = 3Pv_{qs}^e L_M/(4L_s)$, and $\gamma = D(1-s)$ are evaluated at the initial operation condition.

The system has two zeros and three poles. Unlike (13), there are no poles on the origin. Interestingly, the zeros are placed by torque control and HPF designs, and the poles placed by the frequency control design. Although the HPF introduces a pole and zero, it provides ability to specify frequency response to be faster than torque response. Strategic pole placement limits influence of the inertial component and allows return to $T_e^*$ and $Q_s^*$ upon subsidence of response. The frequency response can be tuned via the mix of PI gains for stable and satisfying response characteristic.

## 4 | EXPERIMENTS WITH THE PROPOSED RESPONSE

Tests are performed in this section to evaluate the DFIG frequency response for i) utility-connected and ii) islanding support. The objective of these experiments are to validate capabilities of the proposed controller and to demonstrate an improved use of DFIG inertia in its frequency response. Experiments are performed under several sets of control designs and load-transient conditions. The low-inertia DFIG test system is photographed in Figure 5 and with components and connections as in Figure 1. It consists of an 1800 rpm 7.5 kW DFIG with an 86 kg steel flywheel attached to the rotor shaft, achieving $J = 2.5\,\text{kg}\cdot\text{m}^2$. Electrical parameters and nameplate ratings of the DFIG are available in the Appendix. The generator is driven by a dynamometer using a torque-control mode with constant torque $T_m$ for the duration of study; variation of aerodynamic torque with $\omega_r$ is neglected. The GSC and MSC are controlled by dSPACE ds1103 microcontrollers. More negative $T_e$ and $\Delta\omega_{rm} < 0$ is evidence of a well-regulating inertial response to a load increase; rotor kinetic energy is exchanged to support the electrical load.

### 4.1 | Utility-connected local load support

Response capability is first evaluated by interconnecting with a real local utility, as in Figure 1. In steady-state, the DFIG operates with MPPT power and unity power factor. An event is simulated and the first moments of the response are evaluated. When CB1 is closed, local load is well supported by the high-inertia utility connection provided at the laboratory. Changing the load via CB2 and CB3 creates a transient event observed by the utility and the local DFIG; frequency response is initiated in both.

Pictured in Figure 6 is the DFIG response to local 6.1 kW resistive load addition while $\omega_{rm} = 1630$ rpm (making $P_{MPPT} = 5.9$ kW) for the control variations listed in Table 3. Case A is TQ control alone and B–D are TQ plus FV control. The same TQ control design is used for each case, having the respective closed-loop transfer function poles $s_{pT,Q} = -0.5, -0.5$ rad/s and zeros $s_{zT,Q} = -0.25, -1$ rad/s with LPFs of $\tau_2 = 0.16$ s. For case A, results indicate nearly zero

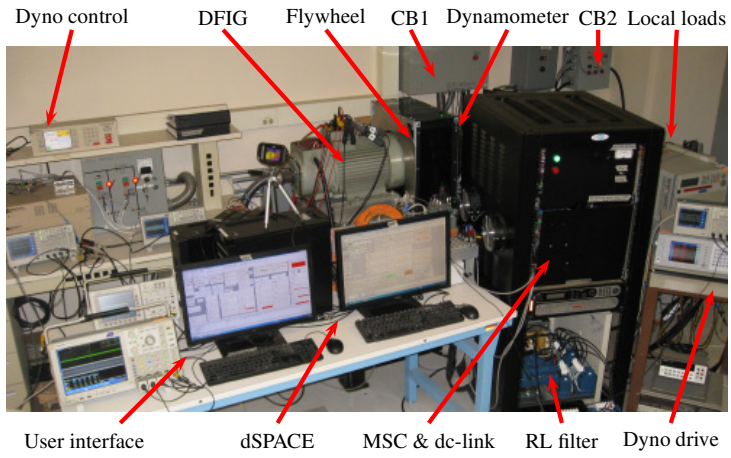


**FIGURE 5** Low-inertia power system test stand with a 7.5 kW DFIG and hub-emulating flywheel, dynamometer, PE converters, and local loads.

**TABLE 3** Tested FV control designs and their grid-connected inertial frequency response.

| Control designs: | A (TQ-only) | B (TQ+FV, slow) | C (TQ+FV, med) | D (TQ+FV, fast) |
|---|---|---|---|---|
| $\tau_6$ (s) | NA | 10 | 5 | 2 |
| **Frequency response results:** | | | | |
| $\Delta f_{e,\,\text{nadir}}$ (mHz) | -7.4 | -2.8 | -4.1 | -3.5 |
| $t$ at $f_{e,\text{nadir}}$ (s) | 0.120 | 0.135 | 0.099 | 0.079 |
| $\Delta\omega_{rm,\,\text{nadir}}$ (rpm) | NA | -102 | -72 | -65 |
| $t$ at $\omega_{rm,\text{nadir}}$ (s) | NA | 6.9 | 4.5 | 3.9 |
| Comment | No grid support | Interferes with others | Interferes less | Good grid support |

frequency response, and actually, $T_e$ indicates slight temporary load rejection. For the tests of B – D, the FV response is made to be faster than the TQ response and (21) is stabilized. The poles and zeros of the FV control closed-loop transfer functions of (19) and (20) are placed so that $s_{pF,V} = -10$ rad/s and $s_{zF,V} = -20$ rad/s with LPFs of $\tau_3 = 0.08$ s. The FV controller follows the grid with the LPF having $\tau_4 = 15$ s. The HPF $\tau_6$ changes the poles and a zero of (21), effecting how the FV control acts on slower grid dynamics. If $\tau_6$ is too large the response can interfere with other utility primary response, evidenced by periods of ACE$\Delta f_e > 0$. Case D has good response; it has small $\tau_6$ and shows mostly ACE$\Delta f_e < 0$, indicating good contribution to the local load-change.

Cases of Figure 6 are shown for an extended duration in Figure 7. With the new FV control added, temporary load support is provided while allowing return to MPPT operation. Evidenced in $\Delta\omega_{rm}$ and ACE$\Delta f_e$, contribution of inertia to the response varies with washout filter $\tau_6$. Observed in $\Delta\omega_{rm}$, smaller $\tau_6$ (case D) allows more control effort and thus faster grid-following transient suppression and recovery; electrical frequency and rotor speed have a higher and faster nadir than without response. Larger $\tau_6$ (case B) extends the duration of response but, again, the relatively fast FV control may interfere with other primary response. Rotor speed and $T_{e,\,\text{MPPT}}$ are restored upon decay of transient response and return to scheduled frequency. The DFIG frequency response is made to be stable and the additional temporary inertial support raises the frequency nadir and shortens its time to occurrence. With the new FV control addition, the electrical transient is more distributed between the electrical and mechanical systems.

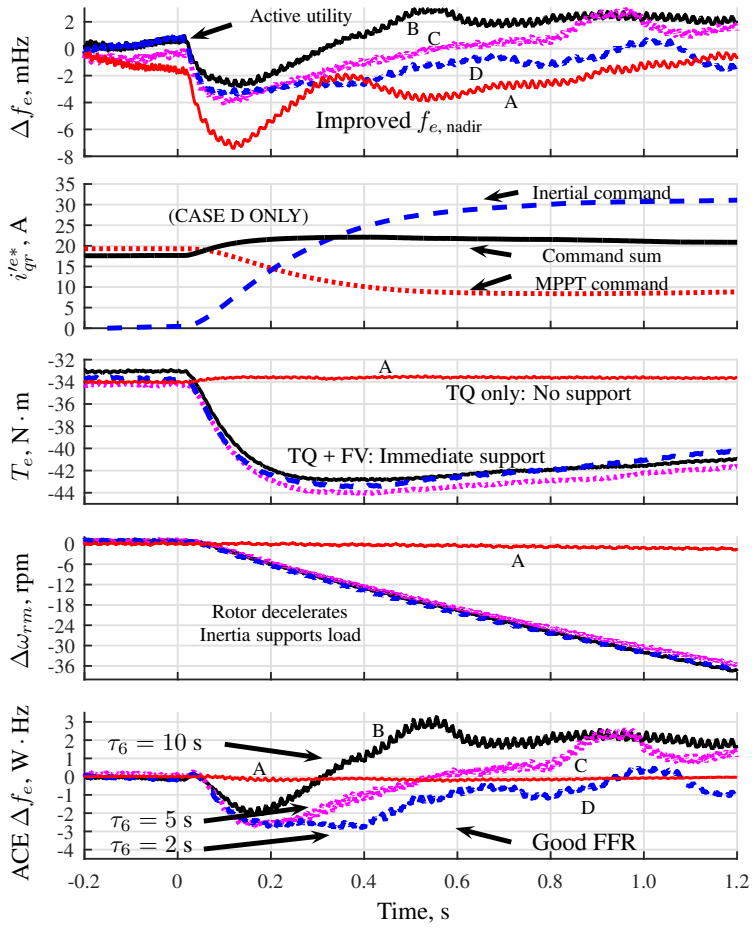


**FIGURE 6** Utility-connected inertial response to local 6.1 kW load increase, for control cases in Table 3.

## 4.2 | Islanding local load support

DFIG inertia can support load even during power-imbalanced islanding conditions. Using a configuration as in Figure 1, when CB1 is opened, the system becomes islanded and the local load is driven only by the DFIG. Although not considered in the theoretical analysis developed with the DFIG in this paper, the GSC also has influence on the frequency response. In this test it is considered with CB4 open and CB5 closed in order to demonstrate the capability. During islanding tests, energy cannot be sourced from anywhere except the physical rotor.

During operation at sub-synchronous rotor, real power is injected into the rotor terminals by the MSC. During operation at super-synchronous speeds the MSC extracts real power from the MCT. Since the GSC handles only up to one-third of the total power in steady-state, and because it is designed to follow applied voltage, it's influence is not expected to be great. Results of the islanding response are provided in Figure 8 for three conditions of varied load and speed.

Cases X, Y, and Z in Figure 8 have the same FV and TQ controller design. The FV poles of (19) are placed so that $s_{pF,V} = -20$ rad/s and $s_{zF,V} = -40$ rad/s with the HPF corner frequency having $\tau_6 = 2$ s. LPFs of the FV control have

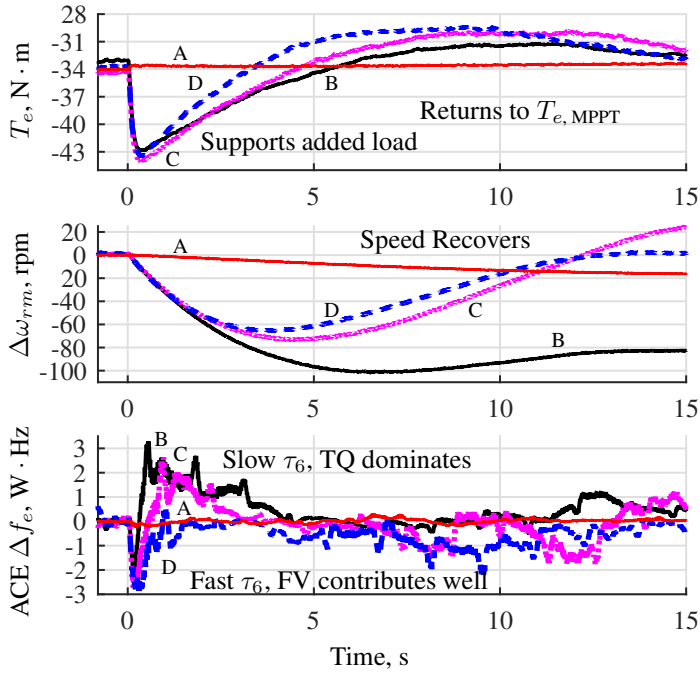


**FIGURE 7** Long-term utility-connected response to local 6.1 kW load increase.

$\tau_3 = 0.08$ s. Response of the TQ controllers are designed with the same parameters as used in the tests of section 4.1, which are relatively slow compared to the FV control. Notice that for all three, the frequency response has similar appearance; i.e. they have the same FV control transfer function design. As time goes on without primary response from other generators, the frequency command, $\omega_e^*$, continues to decline and torque is further increased until the DFIG faults due to rotor over-current. During the gradual decline of $f_e$, other sources should provide primary response to meet the new load requirement. Inertial response with the new FV control maintains the stator voltage with good quality; the transient is nearly indiscernible in $v_{abcs}$.

## 5 | CONCLUSIONS

DFIG wind turbines could contribute to the inertia of power systems, but present controls do not make use of this property. The DFIG controller proposed and tested in this paper showed how it is possible to make a better use of this. It requires no headroom, additional hardware, or communication and is easy to design. Some turbines are presently able to provide "synthetic inertia" which consists of a boost of power in case of frequency decrease. To the contrary of "synthetic inertia", the method of this paper contributes rotor kinetic energy to support load change, not simply frequency change. Experiments using the new controller have shown evidence of sufficient and reliable DFIG inertial support for frequency response in grid-connected and islanding conditions. Compared to the existing state of art, better inertial frequency response is achieved.

Future variations from this control may include saturation of the grid-following FV commands. The turbine would then act to follow the grid with inertial support in normal operation and regulate power and rotor speed to form the grid

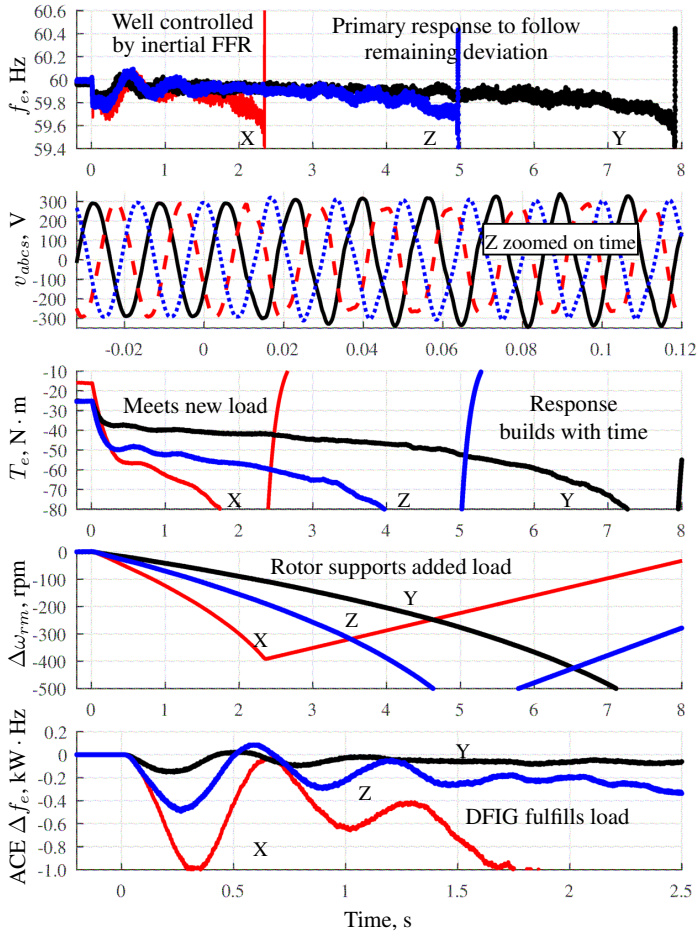


**FIGURE 8** Islanding response of the DFIG. Shown is when X) $\omega_{rm} < \omega_{\text{sync}}$ with CB2 closed and load 1 drawing $2.4P_{\text{MPPT}}$, and also at $\omega_{rm} > \omega_{\text{sync}}$ with Y) CB2 closed drawing $1.17P_{\text{MPPT}}$ and Z) CB3 closed drawing $1.41P_{\text{MPPT}}$.

with constant frequency regulation at the command-value boundaries. Smooth transition from islanding to microgrid topology could also be supported. With the new inertial capability, the DFIG could be thought of in a different way when planning for energy adequacy. Wind turbines could be distributed as system-healing resources that provide regulation of local transients. Additionally, the concept of transient-only control additions could be made in other PE generators too, making use of capacitive or chemical energy storage in transient response as well.

## REFERENCES

[1] Breithaupt T, Herwig D, Hofmann L, Mertens A, Meyer R, Farrokhseresht N, et al. Migrate deliverable 1.1 - Report on systemic issues. TenneT TSO GmbH; 2016.

[2] Miller NW, Shao M, Pajic S, D'Aquila R. Western wind and solar integration study phase 3 - frequency response and transient stability. National Renewable Energy Laboratory; 2014.

[3] Inertia: Basic concepts and impacts on the ERCOT grid. Electric Reliability Council of Texas; 2018.

[4] David N, Wang Z. Physical rotor inertia of DFIG wind turbines for short-term frequency regulation in low-inertia grids. In: 2017 IEEE Power Energy Society General Meeting; 2017. p. 1–5.

[5] Lalor G, Ritchie J, Rourke S, Flynn D, O'Malley MJ. Dynamic frequency control with increasing wind generation. In: IEEE Power Engineering Society General Meeting, 2004; 2004. p. 1715–1720 Vol.2.

[6] State of Reliability 2017. North American Electric Reliability Corporation; 2017.

[7] Haileselassie TM, Torres-Olguin RE, Vrana TK, Uhlen K, Undeland T. Main grid frequency support strategy for VSC-HVDC connected wind farms with variable speed wind turbines. In: 2011 IEEE Trondheim PowerTech; 2011. p. 1–6.

[8] Cardenas R, Pena R, Alepuz S, Asher G. Overview of control systems for the operation of DFIGs in wind energy applications. *IEEE Transactions on Industrial Electronics* 2013 July; 60(7):2776–2798.

[9] Loukarakis E, Margaris I, Moutis P. Frequency control support and participation methods provided by wind generation. In: 2009 IEEE Electrical Power Energy Conference (EPEC); 2009. p. 1–6.

[10] Miller NW, Delmerico RW, Kuruvilla K, Shao M. Frequency responsive controls for wind plants in grids with wind high penetration. In: 2012 IEEE Power and Energy Society General Meeting; 2012. p. 1–7.

[11] Aho J, Buckspan A, Laks J, Fleming P, Jeong Y, Dunne F, et al. A tutorial of wind turbine control for supporting grid frequency through active power control. In: 2012 American Control Conference (ACC); 2012. p. 3120–3131.

[12] Shang L, Hu J, Yuan X, Chi Y. Understanding inertial response of variable-speed wind turbines by defined internal potential vector. *Energies* 2016 Dec; 10(22):1–17.

[13] Zhi D, Xu L. Direct power control of DFIG with constant switching frequency and improved transient performance. *IEEE Transactions on Energy Conversion* 2007 March; 22(1):110–118.

[14] Liu J, Miura Y, Ise T. Comparison of dynamic characteristics between virtual synchronous generator and droop control in inverter-based distributed generators. *IEEE Transactions on Power Electronics* 2016 May; 31(5):3600–3611.

[15] Guan M, Pan W, Zhang J, Hao Q, Cheng J, Zheng X. Synchronous generator emulation control strategy for voltage source converter (VSC) stations. *IEEE Transactions on Power Systems* 2015 Nov; 30(6):3093–3101.

[16] Variani MH, Tomsovic K. Two-level control of doubly fed induction generator using flatness-based approach. *IEEE Transactions on Power Systems* 2016 Jan; 31(1):518–525.

[17] Sharma S, Singh B, Chandra A, Al-Haddad K. Control of doubly fed induction generator in standalone wind energy conversion system. In: 2015 IEEE Industry Applications Society Annual Meeting; 2015. p. 1–8.

[18] Tan Y, Meegahapola L, Muttaqi KM. A suboptimal power-point-tracking-based primary frequency response strategy for DFIGs in hybrid remote area power supply systems. *IEEE Transactions on Energy Conversion* 2016 March; 31(1):93–105.

[19] Naidu NKS, Singh B. Experimental implementation of doubly fed induction generator-based standalone wind energy conversion system. *IEEE Transactions on Industry Applications* 2016 July; 52(4):3332–3339.

[20] Ahmad T, Littler T, Naeem W. An active PID-based inertial control of a doubly-fed induction generator. In: 27th Irish Signals and Systems Conference (ISSC); 2016. p. 1–6.

[21] Noroozi M, Farhangi S. Voltage and frequency stability for control of stand-alone DFIG-based wind turbine using direct voltage control method. In: 14th International Conference on Environment and Electrical Engineering; 2014. p. 85–90.

[22] Liu Y, Jiang L, Wu QH, Zhou X. Frequency control of DFIG-based wind power penetrated power systems using switching angle controller and AGC. *IEEE Transactions on Power Systems* 2017 March; 32(2):1553–1567.

[23] Cheng P, Nian H, Wu C, Zhu ZQ. Direct stator current vector control strategy of DFIG without phase-locked loop during network unbalance. *IEEE Transactions on Power Electronics* 2017 Jan; 32(1):284–297.

[24] Fazeli M, Holland P. Universal and seamless control of distributed resources-energy storage for all operational scenarios of microgrids. *IEEE Transactions on Energy Conversion* 2017 Sept; 32(3):963–973.

[25] Li Y, Xu Z, Ostergaard J, Hill DJ. Coordinated control strategies for offshore wind farm integration via VSC-HVDC for system frequency support. *IEEE Transactions on Energy Conversion* 2017 Sept; 32(3):843–856.

[26] Erlich I, Korai A, Neumann T, Zadeh MK, Vogt S, Buchhagen C, et al. New control of wind turbines ensuring stable and secure speration following islanding of wind farms. *IEEE Transactions on Energy Conversion* 2017 Sept; 32(3):1263–1271.

[27] Frequency response standard background document. North American Electric Reliability Corporation; 2012.

[28] Milano F, Dörfler F, Hug G, Hill DJ, Verbič G. Foundations and challenges of low-inertia systems. In: 20th Power Systems Computation Conference; 2018. p. 1–25.

[29] Frequency response - issue paper. California Independent System Operator; 2015.

[30] Std. BAL-001-2 Real power balancing control performance. North American Electric Reliability Corporation; 2016.

[31] Luna A, Citro C, Gavriluta C, Hermoso J, Candela I, Rodriguez P. Advanced PLL structures for grid synchronization in distributed generation. In: 2012 EA4EPQ International Conference on Renewable Energies and Power Quality; 2012. p. 1–10.

[32] Krause PC, Wasynczuk O, Sudhoff SD. *Analysis of electric machinery*. IEEE Press; 1995.

## A | DFIG PARAMETERS

The machine under test is a 6-pole wound rotor induction machine (part no: YZR 160M2-6), which has the following nameplate ratings for a Δ-Y connection: $f = 60$ Hz, $V_s = 208$ $V_{LL}$, $V_r = 195$ $V_{LL}$, $I_s = 31$ A, $I_r = 26$ A, and $P_{shaft} = 7.5$ kW.

The per-phase equivalent circuit parameters were obtained following IEEE Standard 112-2004. The per-phase equivalent circuit machine parameters are $r_s = 0.1593$ Ω, $r'_r = 0.0869$ Ω, $L_{ls} = 1.9$ mH, $L'_{lr} = 1.9$ mH, and $L_M = 17.1$ mH.